THE ASTROPHYSICAL JOURNAL, 436:355–367, 1994 November 20

EQUILIBRIUM STRUCTURE OF SOLAR MAGNETIC FLUX TUBES: ENERGY TRANSPORT WITH MULTISTREAM RADIATIVE TRANSFER

S. S. HASAN[1] AND W. KALKOFEN
Harvard-Smithsonian Center for Astrophysics, 60 Garden Street, Cambridge MA 02138
Received 1993 June 4; accepted 1994 January 31

ABSTRACT

We examine the equilibrium structure of vertical intense magnetic flux tubes on the Sun. Assuming cylindrical geometry, we solve the magnetohydrostatic equations in the thin flux-tube approximation, allowing for energy transport by radiation and convection. The radiative transfer equation is solved in the six-stream approximation, assuming gray opacity and local thermodynamic equilibrium. This constitutes a significant improvement over a previous study, in which the transfer was solved using the multidimensional generalization of the Eddington approximation. Convection in the flux tube is treated using mixing-length theory, with an additional parameter α, characterizing the suppression of convective energy transport in the tube by the strong magnetic field. The equations are solved using the method of partial linearization. We present results for tubes with different values of the magnetic field strength and radius at a fixed depth in the atmosphere. In general, we find that, at equal geometric heights, the temperature on the tube axis, compared to the ambient medium, is higher in the photosphere and lower in the convection zone, with the difference becoming larger for thicker tubes. At equal optical depths the tubes are generally hotter than their surroundings. The results are comparatively insensitive to α but depend upon whether radiative and convective energy transport operate simultaneously or in separate layers. A comparison of our results with semiempirical models shows that the temperature and intensity contrast are in broad agreement. However, the field strengths of the flux-tube models are somewhat lower than the values inferred from observations.

Subject headings: MHD — radiative transfer — Sun: atmosphere — Sun: magnetic fields

1. INTRODUCTION

It is well known that the surface magnetic field of the Sun occurs in the form of discrete flux tubes with field strengths typically in the 1–2 kG range (see review by Stenflo 1989 and references therein). High-resolution observations of the solar photosphere have revealed considerable information about the properties of magnetic elements (Dunn & Zirker 1973; Mehltretter 1974; Muller 1983; Title et al. 1992). Recently, several semiempirical models have been developed for intense flux tubes, using Fourier transform–based observations of high spectral resolution (e.g., Keller et al. 1990; Zayer et al. 1990; see also the review by Solanki 1990). These have helped greatly in providing much insight into physical conditions within flux tubes. In order to make meaningful comparisons with observations, it is important that the theoretical models achieve a level of sophistication such that they capture the essential physics of processes occurring in intense flux tubes. The purpose of this paper is to propose refinements which would contribute in this direction.

Our investigation is a continuation of earlier work by Hasan (1988, hereafter Paper I) and Kalkofen et al. (1986) on the equilibrium structure of intense flux tubes. In Paper I, self-consistent model calculations were presented for the structure of a vertical thin flux tube, taking into account energy transport by radiation and convection. The motivation of these calculations was mainly to provide a "time-averaged" model atmosphere in a flux tube (neglecting flows), which could also be used as the initial state in stability and time-dependent calculations. The spirit of this paper is similar to that of Paper I, except that we used a more refined treatment of radiative transfer in the present analysis.

Magnetostatic models of intense flux tubes were first developed by Spruit (1976). The temperature structure inside the flux tube was determined by solving a heat transport equation (in two dimensions) with a diffusion coefficient that included contributions from radiation and convection. These models were not self-consistent because the momentum and energy equations were treated separately. Nevertheless, they provided a qualitative understanding of flux tubes and also demonstrated that the horizontal size (i.e., tube radius) and heat exchange with the ambient medium play an important role in determining the temperature structure of the tube. The influence of radiative transfer on the thermal structure of flux tubes was examined by Ferrari et al. (1985), Kalkofen et al. (1986, 1989), and Fabiani Bendicho, Kneer, & Trujillo Bueno (1992). However, convective energy transport was neglected in these studies. The contributions due to both radiative transfer (in the Eddington approximation) and convection were considered in Paper I. Self-consistent magnetostatic models of flux tubes in cylindrical geometry with rotational symmetry were constructed by Steiner & Stenflo (1989). These had the advantage of providing a more realistic treatment of the horizontal temperature and field variation. However, they were limited (similar to the other models mentioned above) due to the neglect of convective energy transport. Recently, Pizzo, MacGregor, & Kunasz (1993) have attempted to incorporate the convection zone in two-dimensional transfer calculations. Although this allows them to extend the previous calculations to deeper layers, their treatment has the drawback that the temperature structure is a priori specified in the convection

[1] Postal address: Indian Institute of Astrophysics, Sarjapur Road, Bangalore 560034, India.

zone, and the deep and shallow layers are essentially thermodynamically decoupled. Also, the transition layer, in which both radiative and convective transport operate simultaneously, is excluded in these calculations. We shall show that this can introduce errors in the computed temperature profiles and also on the intensity contrast.

In the present investigation, we use a quasi–two-dimensional treatment to model radiative transfer in a flux tube. The advantage of this approach is that it incorporates heat exchange between the tube and the ambient medium using a more refined treatment of transfer and at the same time allows for a continuous transition from radiative transport in the photospheric layers to convective transport in the deeper regions. We should point out that there are several other studies which have modeled flux tubes using, however, a time-dependent approach. For instance, Hasan (1984, 1985, 1990, 1991) has examined the structure of a tube when dynamical effects are taken into account, within the framework of the thin flux-tube approximation. Time-dependent two-dimensional slab models for flux sheaths have also been constructed by Deinzer et al. (1984), Grossman-Doerth, Knölcker, & Schüssler (1989), Knölker, Schüssler, & Weisshaar (1988), and Knölker & Schüssler (1988). The time-dependent studies reveal the presence of oscillatory flows within the tubes and downflows in their immediate periphery. However, since the magnitude of these flows is quite small, it seems reasonable as a first approximation to neglect their effect in order to obtain an "average" atmosphere in a tube, in the same spirit as Paper I. Furthermore, the time-dependent calculations, particularly with a realistic treatment of radiative transfer, require enormous amounts of computer time. Using the technique that we describe in the ensuing sections, it is possible to construct flux-tube models for a large range of parameters with modest computing requirements.

The plan of the paper is as follows: in § 2, we describe the model and present the relevant equations. Section 3 discusses the numerical procedure. The results are presented in § 4, followed by a discussion in § 5. Finally, in § 6, the main conclusions of the study are summarized.

2. EQUATIONS

The model that we use has been described in detail in Paper I; however, for the sake of clarity we briefly summarize its main features. We consider a vertical flux tube of circular cross section and adopt a cylindrical coordinate system. Furthermore, we assume axial symmetry, and for simplicity adopt the thin flux-tube approximation to treat the magnetostatic equations. To lowest order, the relevant equations for a thin flux tube are

$$\frac{dp}{dz} = \rho g \,, \tag{1}$$

$$p + \frac{B^2}{8\pi} = p_e \,, \tag{2}$$

$$\nabla \cdot \boldsymbol{F} = 0 \,, \tag{3}$$

where z, the vertical coordinate is measured positive into the Sun, ρ is the density of fluid in the tube, p is the pressure, B is value of the magnetic field, $\boldsymbol{F}$ is the energy flux, and the subscript e refers to the external atmosphere. The quantities, which refer to the atmosphere inside the flux tube, are evaluated on the tube axis. The radius of the tube a is determined from the magnetic flux conservation condition,

$$Ba^2 = \Phi \,, \tag{4}$$

where Φ is the magnetic flux, which is constant with z. The temperature T is related to the pressure and density through the ideal gas law,

$$p = \rho RT/\mu_g \,, \tag{5}$$

where R and μ_g are the gas constant and mean molecular weight, respectively.

2.1. *Energy Transport*

Following Paper I, we assume that energy transport occurs solely through radiation and convection (we neglect extra heating). We use the same expression as in Paper I for the convective flux, which was obtained using a mixing-length formalism (Cox & Giuli 1968, pp. 281–325) with an additional parameter α. The latter characterizes the suppression of convection in the tube due to the strong magnetic field. Following Spruit (1976), we neglect the radial component of the convective energy flux within the tube. Further details can be found in Paper I.

We now present details of the radiative transfer. Unlike Paper I, we do not adopt the Eddington approximation, but instead consider the mean radiation field to have contributions from rays emanating in several directions. We retain the assumptions of LTE and a gray atmosphere. In this approximation, the transfer equation for a single ray in a plane corresponding to a fixed aximuthal angle ϕ is (e.g., Mihalas 1978)

$$\mu_m^2 \frac{\partial^2 J_m}{\partial \tau^2} = J_m - S \quad (m = 1, \ldots M) \,, \tag{6}$$

where μ_m is the cosine of the angle that the ray makes with the z-axis, τ denotes the vertical optical depth, S is the source function, m is an index denoting a specific ray, M is the total number of rays, and $J_m(\phi)$ is related to the specific intensity $I(\mu_m, \phi)$ in the direction (μ_m, ϕ) through

$$J_m(\phi) = \frac{I(\mu_m, \phi) + I(-\mu_m, \phi)}{2} \,. \tag{7}$$

We neglect scattering, in which case S becomes the Planck function. The geometrical and optical depths are related through

$$d\tau = \kappa \, dz \,, \tag{8}$$

where κ is the Rosseland mean opacity per unit distance.

The boundary conditions used with equation (6) are no incoming radiation at the top boundary and a specific intensity in the upward direction at the lower boundary given by the diffusion approximation. These choices are reasonable if the upper boundary of the atmosphere is situated in layers where the optical depth is very small and the lower boundary is located sufficiently deep in the atmosphere where the optical depth is very large. Following Mihalas (1978), the boundary conditions can be written as

$$\mu_m \frac{\partial J_m}{\partial \tau} = J_m \quad (m = 1, \ldots M), \quad \tau = 0 \,, \tag{9}$$

$$\mu_m \frac{\partial J_m}{\partial \tau} = -J_m + I_m^+ \quad (m = 1, \ldots M), \quad \tau \gg 1 \,, \tag{10}$$

where

$$I_m^+ = S + \mu_m \frac{\partial S}{\partial \tau} \tag{11}$$

is the specific intensity entering in the direction m at the lower boundary. The mean intensity and J and radiative flux $\boldsymbol{F}_R$ are, respectively,

$$J = \frac{1}{4\pi} \int_0^{2\pi} d\phi \int_{-1}^{1} d\mu\, I(\mu, \phi) , \tag{12}$$

$$\boldsymbol{F}_R = 4\pi \int_0^{2\pi} d\phi \int_{-1}^{1} d\mu\, \boldsymbol{n} I(\mu, \phi) . \tag{13}$$

The mean intensity and radiative flux are related through

$$\nabla \cdot \boldsymbol{F}_R = 4\pi\kappa\rho(S - J) . \tag{14}$$

Substituting equation (13) into equation (3), and remembering that the convective flux has only a vertical component, we find that the energy equation becomes

$$\frac{\partial F_{c,z}}{\partial z} - 4\pi\kappa\rho(J - S) = 0 , \tag{15}$$

where $F_{c,z}$ is the z component of the convective flux. We assume that the total vertical flux is specified at the lower boundary.

3. NUMERICAL PROCEDURE

The numerical procedure that we adopt to construct the equilibrium atmosphere is based on the partial linearization method of Auer & Mihalas (1968) as modified by Gustafsson (1971). Details can be found in Paper I. Starting from an assumed atmosphere, the method basically uses Newton-Raphson iteration to calculate corrections to various quantities until convergence is achieved.

For reasons of consistency, we first use this method to construct the atmosphere outside the tube. Since there are differences in the way that the external and internal atmospheres are calculated, it is convenient to treat them separately. We shall confine ourselves mainly to the treatment of radiative transfer. The formulation for treating convection is the same as in Paper I.

3.1. *External Atmosphere*

We assume that the external atmosphere is plane parallel, so that the spatial variation is solely with respect to z. We disregard the influence of the flux tube on the ambient medium. Equation (3) can be integrated to give

$$F_{R,z}^{(e)} + F_{c,z}^{(e)} = F_\odot , \tag{16}$$

where $F_\odot$ denotes the constant solar flux. It is easy to show from equation (13) and the transfer equation that the vertical radiative flux for a plane-parallel atmosphere is given by

$$F_{R,z} = 4\pi \sum_{m=1}^{M} a_m \mu_m^2 \frac{\partial J}{\partial \tau_m} , \tag{17}$$

where the integration over polar angle has been replaced by a quadrature-based formula with weights a_m (Chandrasekhar 1960). The azimuthal integration in this case is trivial. We shall henceforth drop the subscript z and tacitly assume that the flux refers solely to the vertical component.

We linearize equations (1), (6), and (13) with respect to T, p, and J_m similarly as in Paper I. Let us divide the integration region in the z-direction into a grid with points located at z_k; $k = 0, 1, \ldots N$. Using finite differences to approximate the derivatives, the equations can be cast in the following block tridiagonal form for the corrections δJ_m, δT and δp:

$$\begin{pmatrix} B_0 & -C_0 & . & . & . & . \\ A_1 & -B_0 & C_1 & . & . & . \\ . & . & . & . & . & . \\ . & . & . & -A_{N-1} & B_{N-1} & -C_{N-1} \\ . & . & . & . & -A_N & B_N \end{pmatrix} \begin{pmatrix} X_0 \\ X_1 \\ . \\ X_{N-1} \\ X_N \end{pmatrix} = \begin{pmatrix} D_0 \\ D_1 \\ . \\ D_{N-1} \\ D_N \end{pmatrix} , \tag{18}$$

where A_k, B_k, C_k are matrices of order $(M + 2) \times (M + 2)$, D_k and X_k are column vectors of order $M + 2$ with $X_k = (\delta J_1, \delta J_2, \ldots \delta J_M, \delta T, \delta p)^T$. The detailed structures of the block matrices are similar to those given in Appendix A of Paper I.

Equation (18) is solved using standard methods to determine the corrections X_k, $k = 0, 1, \ldots N$ for a fixed vertical flux, assuming a specified pressure p_0 at $z = z_0$ and the discretized form of the boundary conditions, equations (9)–(10). Starting from an initial guess atmosphere, which we take to be the combined models of Vernazza, Avrett, & Loeser (1976) and Spruit (1977, pp. 26–34), equation (18) is solved until the corrections become sufficiently small, similar to the procedure followed in Paper I. The Saha equation is solved after each iteration to determine the degree of ionization and various thermodynamic quantities such as the mean molecular weight and specific heats. We determine the opacity by combining the tables of Kurucz (1992) for the upper layers of the atmosphere with those of Rogers & Iglesias (1992) for the deeper regions.

3.2. *Flux-Tube Atmosphere*

The atmosphere in the flux tube is also generated iteratively. We initially assume that the internal and external temperatures are equal at the same geometric level. The density and pressure inside the tube are lower at each height than the ambient value by the factor $\beta/(\beta + 1)$, where $\beta = 8\pi p/B^2$. For the starting solution β is almost constant with depth. The mean intensity on the tube axis is determined by solving, at various depths, the transfer equation for several rays at different angles. We now describe the method used for calculating the mean intensity inside the flux tube.

3.2.1. *Mean Radiation Intensity on the Tube Axis*

In order to determine the mean radiation intensity on the axis of the tube, we need to solve the transfer equation along several rays, which emanate from the external atmosphere and traverse the tube at different inclinations. In the most general case, the solution of the transfer equation can be cumbersome, but it becomes tractable if we assume that the radiation field possesses azimuthal symmetry about the tube axis. A useful way to resolve the angular variation of the radiation field is to solve the transfer equation in several planes, tangent to various concentric radial shells, about the tube axis, similar to that used by several authors (e.g., Steiner & Stenflo 1989; Stone, Mihalas, & Norman 1992). We first describe the method for solving the transfer equation in a single plane or flux sheath, whose axis is parallel to the tube axis. In each flux sheath, we

have to take into account the fact that the ray path includes both the internal and external atmospheres.

We use a ray construction, in which all rays pass through the flux sheath axis. Consider a single ray coming from the bottom of the external atmosphere and crossing the axis. Typically, this ray will have two intersections with the tube boundary. In order to determine J_m at a fixed level on the axis, we need to know the source function S and opacity κ at each point along the ray. In the external atmosphere, S and κ depend only on z, whereas within the sheath they depend on both z and x, the horizontal distance from the axis. We assume that inside the tube, S and κ vary linearly with x from their values on the axis to those in the external medium. Once J_m is determined in this fashion by solving the discretized form of equation (6), along with the boundary conditions given by equations (9) and (10), the mean intensity on the axis of the plane J is found from the quadrature,

$$J = \sum_{m=1}^{M} a_m J_m .$$

At points close to the top and bottom boundaries, there is only one intersection with the tube wall of a ray crossing the axis. This occurs when a ray reaches the levels z_0 or z_N inside the tube. For such rays, the solutions proceed similarly as before, except that the boundary conditions on J_m are now applied inside the tube.

The off-axis mean intensity can be determined using a method similar to the short characteristic method (Kunasz & Auer 1988). Having obtained the radiation intensity on several tangent planes, it is a simple matter to do the azimuthal integration, which can be reduced to a quadrature. Following O. Steiner (1993, private communication), we use a trapezoidal rule to carry out the azimuthal integration.

In this paper, we are basically interested only in determining the mean intensity on the axis of the tube. To resolve the azimuthal variation, we follow Stone et al. (1992) and consider a set of planes very close to the tube axis. It turns out that for thin flux tubes, like the ones we are considering, the degree of azimuthal anisotropy close to the axis of the tube is extremely small (less than 3%), so that it is sufficient, in the present context, to treat a single planar cut through the tube axis, about which the radiation field can be regarded as symmetric. This also implies that the radial component of the radiative flux $F_{R,r}$ is zero on the axis. Away from the axis, $F_{R,r}$ is in general nonzero. However, we do not compute its value off-axis.

3.2.2. *Temperature and Pressure on the Tube Axis*

In order to determine the temperature and pressure on the tube axis, we linearize equations (1) and (15) with respect to T and p, assuming that J is known. We take the upper boundary of our integration domain to lie in layers where there is no convection, so that the energy equation (15) reduces to

$$J - S = 0 .$$

The lower boundary is taken to lie in optically thick layers where the diffusion approximation holds and $J - S \to 0$, and equation (15) integrates to

$$F_c = F_{\rm bot} ,$$

where $F_{\rm bot}$ is the vertical convective flux at the lower boundary of the tube. We take $F_{\rm bot} = \alpha F_{\odot}$, where α denotes the convective efficiency parameter within the tube (following Paper I, we assume that α is constant). At the top boundary we assume that the pressure is specified as follows:

$$p_0 = \frac{\beta_0}{\beta_0 + 1} p_e ,$$

where β_0, the value of β at $z = z_0$, is an input parameter. Thus B_0 is automatically fixed as well by equation (2).

The linearized equations for the flux tube have the same structure as equation (18), except that A_k, B_k, C_k are 2×2 matrices, and D_k and X_k are column vectors of order 2. The latter have the form $X_k = (\delta T_k \, \delta p_k)^T$. Once the temperature and pressure are obtained, the magnetic field and radius are determined from equations (2) and (4), respectively. We then calculate the state of ionization and hence various thermodynamic quantities. Opacities are found as before by interpolating from tables. The transfer equation is again solved to determine J, and the procedure is repeated until convergence is achieved. In practice, about 20 iterations are generally sufficient to reduce the maximum temperature correction below 1 K.

4. RESULTS

We now present model calculations based on the numerical procedure described in the previous section. For the sake of self-consistency, we first use our method to generate the atmosphere in the external atmosphere. We use the same formulation of mixing-length theory as in Paper I to treat convection. The upper and lower boundaries of our computational domain are taken at $z = -500$ km and $z = 2000$ km, respectively. We used 250 grid points with a uniform spacing of 10 km, which is found adequate to resolve the steepest spatial gradients.

4.1. *Temperature Variation with Depth in the External Atmosphere*

Figure 1 shows the temperature variation with depth in the external medium for various angle approximations. The numbers beside the curves denote the total number of angles used in the transfer. We find that the curves for three or more angles are indistinguishable. The filled inverted traingles correspond to the level where the optical depth is unity. The maximum difference in temperature between the three- and four-angle approximations is 10 K and occurs at $z \approx -100$. In view of this, we found that the three-angle or six-stream approximation was adequate in the treatment of radiative transfer. For $z < 0$, convection is absent and the atmosphere is in radiative equilibrium. Below $z = 0$, the criterion for the onset of convection is satisfied, and both radiative and convective energy transport mechanisms are present. At about $z = 50$ km (corresponding to a vertical optical depth of about 5; see Fig. 2), the opacity becomes sufficiently large that radiative transport becomes inefficient compared to convection. Incidentally, the transition from pure radiative to pure convective transport occurs smoothly in a way that the total vertical flux is conserved (better than a relative accuracy of 0.1%).

4.2. *Flux-Tube Geometry and Ray Construction*

Figure 2 depicts a vertical planar section of a tube (with the tube boundary denoted by *thick solid lines*), corresponding to $\alpha = 0.2$, $\beta_0 = 1.0$, and $a(0) = 50$ km, where $a(0)$ is the radius of the tube at $z = 0$. Unless otherwise stated, these will henceforth

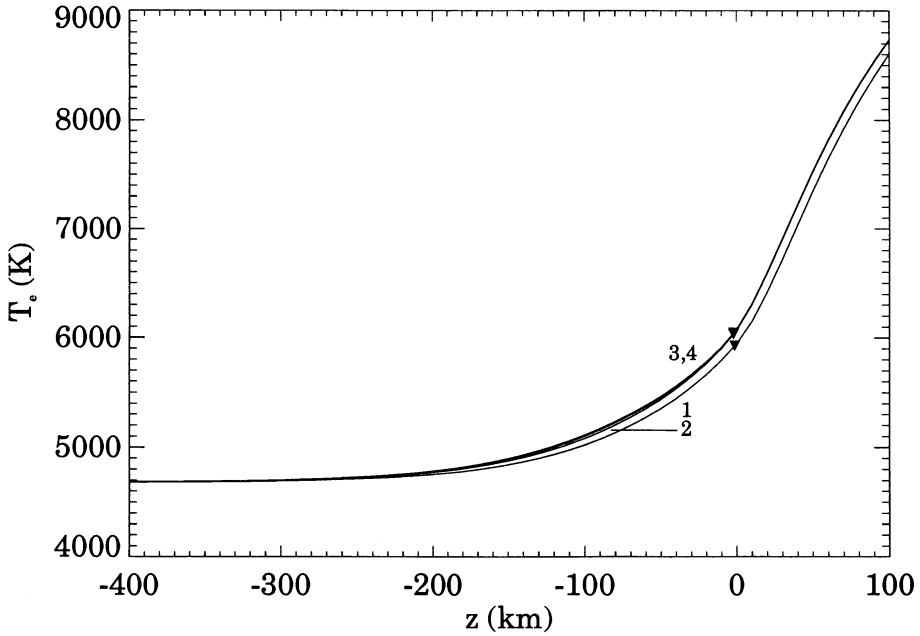

FIG. 1.—Temperature as a function of z in the external atmosphere for various angle approximations. The numbers beside the curves denote the total number of angles used in the radiative transfer equation. The filled inverted triangles denote the levels in the external atmosphere where the optical depth is unity.

be the default parameters for all figures. The thin solid and dotted lines show segments, inside the tube, of the shallowest and steepest rays used in the six-stream (three-angle) approximation; the intermediate ray has been omitted. Of course, the full ray construction involves extending the rays until they reach the top and bottom boundaries. We have not shown in the figure the ray segments lying outside the tube, and also we treat only rays passing through the tube axis. Since we have assumed symmetry about the tube axis, only one of each pair of rays at a given angle is used in the calculation. The axes on the right denote the vertical optical depths inside the tube and in the external atmosphere, respectively. Owing to the reduced internal gas density, the optical depth scale inside the flux tube is shifted downward with respect to that in the ambient medium. These scales can be used for determining the relation between the geometric and optical depths.

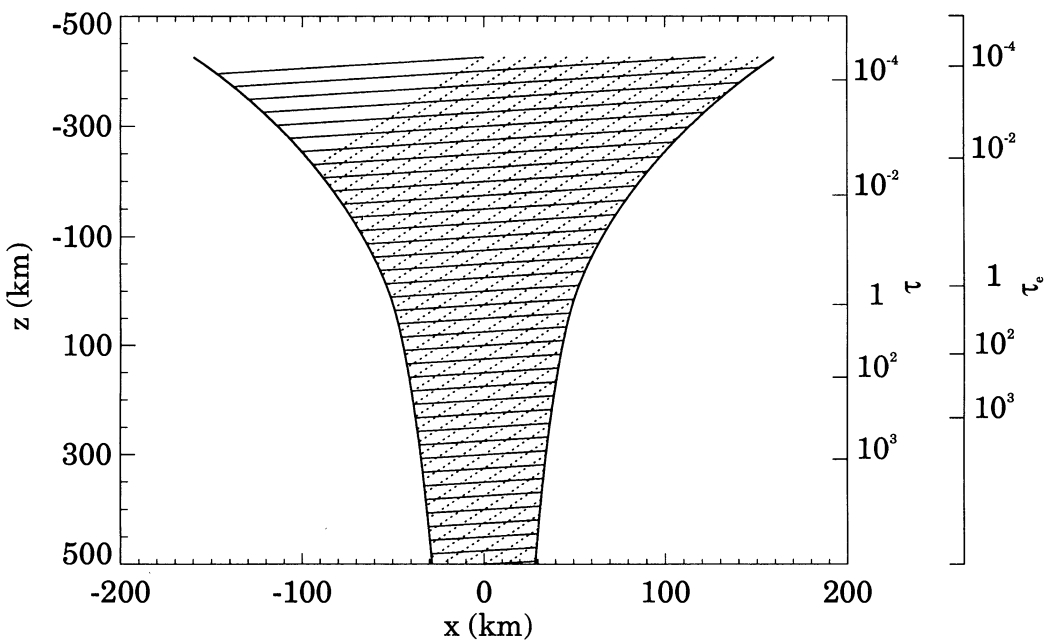

FIG. 2.—Vertical cross section of the tube for $\alpha = 0.2$, $\beta_0 = 1.0$, and $a(0) = 50$ km (the default parameters). The thick solid lines denote the tube boundary, and x denotes the horizontal coordinate with respect to the tube axis. Thin and solid dotted lines show the ray segments, inside the tube, of the shallowest and steepest rays used in the three-angle approximation to the transfer equation. The axes on the right correspond to the vertical optical depths on the tube axis and in the external atmosphere, denoted by τ and τ_e, respectively.

4.3. *Temperature Variation with Depth on the Flux-Tube Axis*

Figure 3 shows the variation with depth z of the tube temperature T_i (*solid lines*) and its difference with the external temperature $\Delta T = T_i - T_e$ (*dashed lines*), assuming default values for the various parameters. The curves denoted by 3 correspond to three-angle (or six-stream) approximation in the computation of the mean radiation intensity. For purposes of comparison, we also present solutions (curves annotated as "Ed") calculated on the basis of the generalized Eddington approximation, used in Paper I (for consistency we have repeated the calculations of Paper I, using the same opacities and abundances as those used in the present study). The external atmosphere for the latter solution corresponds to the single ray (two-stream approximation), shown in Figure 1. For purposes of focusing on the effect of the transfer on the temperature structure in the tube, we have not added an additional heating term as was done in Paper I. Clearly, the generalized Eddington approximation leads to an atmosphere which is essentially isothermal in the horizontal direction with respect to the ambient medium, for $z < 0$, whereas the present calculation shows that in these layers, the temperature on the tube axis is higher than that in the external atmosphere with ΔT decreasing upward in the atmosphere. It appears that the previous treatment overestimates lateral heat exchange in the upper photosphere but underestimates it in the subphotospheric regions. Our results also show that, close to the upper boundary, the external and internal temperatures tend to become the same. The reason for this behavior is that in such layers, a point on the tube axis is bathed mainly in radiation from the external medium, since the optical path length of the rays intercepted by the flux tube is very small, $\delta\tau \sim 10^{-3}$ (see Fig. 2). These results are influenced to some extent by our assumption that the external atmosphere is unaffected by the tube (see Kalkofen et al. 1989). In the layers just above $z = 0$, the flux tube is hotter than the external atmosphere at the same geometric level. The reason for this phenomenon is that, because of the lower density in the tube and the exponential growth of density and hence opacity with depth, the reduced specific intensity of radiation from shallower layers is more than compensated by the increased intensity (along the same ray) from deeper layers (see Kalkofen et al. 1986). This effect increases with tube radius until the increased radiative flux in the flux tube in the horizontal and vertical direction is felt by the external medium and results in a lower temperature than that of the undisturbed atmosphere. In the subphotospheric part of the atmosphere ($z < 0$), the effect of convection with a reduced efficiency is felt, which lowers the temperature gradient with respect to vertical optical depth, and hence $T_i < T_e$ at the same geometric level.

4.4. *Influence of Radius on Temperature and Vertical Flux in the Tube*

Figure 4 shows the depth variation in the tube of the temperature T_i (*solid lines*) and the total vertical flux F_{tot} (*dashed lines*) for different values of the tube radius, parameterized by $a(0)$. The external temperature T_e is also shown for comparison as a heavy dashed curve. The filled inverted triangles on the solid curves denote the optical depth unity levels within the flux tube. As pointed out earlier, the flux tube is hotter and cooler, respectively, than the external medium for $z < 0$ and $z > 0$. Figure 4 shows that this difference is larger for thicker tubes, but it should be noted that the effect of the flux tube on the external medium has been neglected here. In the layers $z < 0$, the increase of T_i with $a(0)$ can be understood by looking at the ray construction in Figure 2. As the thickness of the tube increases, the influence of the more vertical rays, emanating from the deep hot layers, is more pronounced on the temperature on the tube axis than that of the horizontal rays from cooler regions. For $z > 0$, we have already noted that the internal temperature is reduced with respect to the surrounding atmosphere. Now in this region, it is the shallow rays coming from cooler layers which dominate the temperature structure,

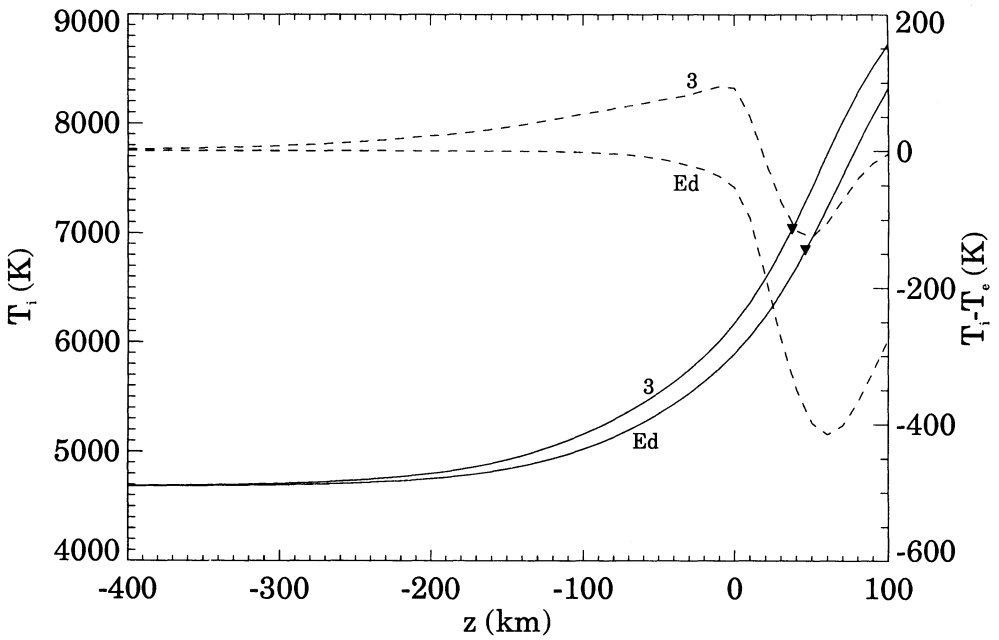

FIG. 3.—Variation of T_i (*solid lines*) and $T_i - T_e$ (*dashed lines*) with z for the default parameters. The labels 3 and Ed denote the three-angle and the generalized Eddington approximations, respectively, in the transfer equation. The filled inverted triangles denote the levels in the tube where the vertical optical depth is unity. Note that no additional heating has been used in the energy equation.

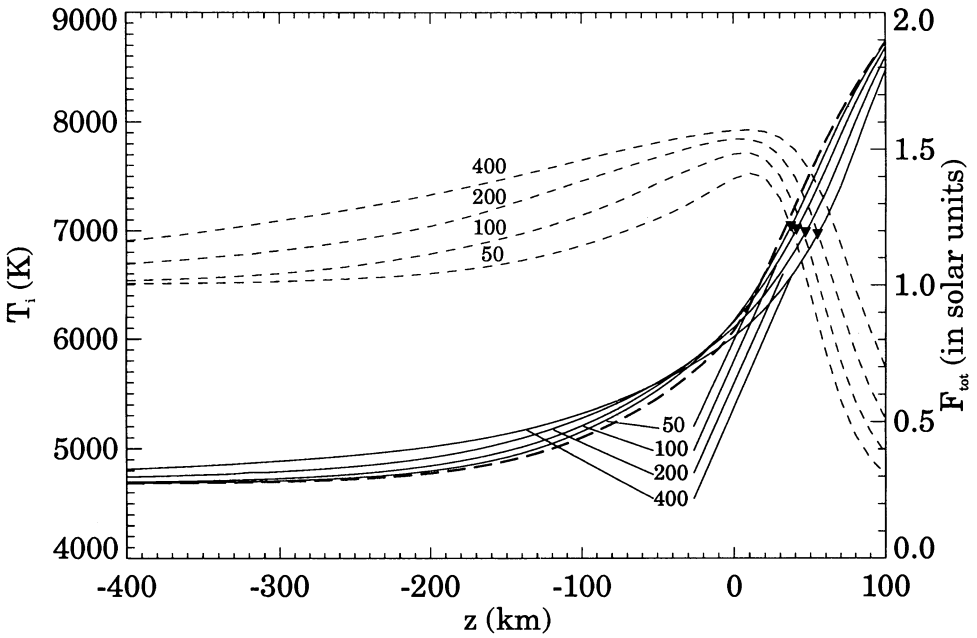

FIG. 4.—Variation of T_i (*solid lines*) and F_{tot} (*dashed lines*) with z for different values of $a(0)$, which are used to label the curves, assuming $\alpha = 0.2$ and $\beta_0 = 1.0$. The thick dashed curve corresponds to the temperature distribution in the external atmosphere. The filled inverted triangles denote the levels in the tube where the vertical optical depth is unity.

since the opacity increases very rapidly with depth in this region. This also is consistent with the $\tau = 1$ levels moving downward or the Wilson depression increasing with $a(0)$. For very large optical depths, radiative energy transport becomes negligible, and the internal temperature is determined solely by convective energy transport. Since we have assumed that the latter is independent of $a(0)$, the various T_i curves eventually merge with one another.

Let us now consider the behavior of the vertical component of the total flux F_{tot}. Since the convective flux is zero for $z < 0$ and is very small in the subphotospheric layers, F_{tot} can essentially be regarded as the vertical radiative flux $F_{R,z}$. The first point to note is that this flux is not constant with z, reflecting the fact that we have a two-dimensional medium with a horizontal temperature stratification. We also see that increasing the tube radius leads to a larger vertical radiative flux, due mainly to a lowering of the Wilson depression for thicker tubes.

4.5. *Influence of β_0 on Temperature and Field Strength in the Tube*

Figure 5 shows the variation with internal vertical optical depth of the temperature T_i on the tube axis (*solid lines*) for different values of β_0, assuming $a(0) = 50$ km. The variation of T_e with optical depth (in the external atmosphere) is also shown as a heavy dashed line. The filled inverted triangles denote the location of $z = 0$. From the definition of β_0, it is clear that the smallest value of β_0 corresponds to the strongest magnetic field strength. The main effect of varying β_0 manifests itself through a change of the internal gas density. The smaller the value of β_0, the greater is the reduction of ρ inside the tube with respect to the ambient value. The reduced density leads to the vertical optical depth scale in the tube being shifted downward with respect to the external medium, so that $T_i > T_e$ at equal τ. Decreasing β_0 leads to a higher internal temperature at the same optical depth. Also, it should be noted that as β_0 decreases, the depth at which the optical depth is unity in the flux tube increases. This is evident from the location of the filled inverted triangles.

The dashed curves show the variation of B with τ. We assume that the pressure and magnetic field at the top boundary are specified. As expected, the magnetic field varies monotonically with τ, with the value at a fixed optical depth increasing with a decrease in β_0.

4.6. *Variation of F_{tot} and β with z for Different β_0*

Figure 6 shows the variation with z of the total vertical flux F_{tot} on the axis of the tube (*solid lines*) and $\beta(z)$ (*dashed lines*) for various values of β_0 assuming, as before, $a(0) = 50$ km and $\alpha = 0.2$. Let us first consider the behavior of F_{tot}. In the deep layers ($z \gg 0$), where the opacity is very high, the main contribution to F_{tot} comes from the convective flux, which is assumed to be independent of β_0. However, in the shallower layers, convection becomes ineffective, and radiative energy transport dominates. Due to the reduced opacity in the tube (as a result of the density reduction), radiation from the external atmosphere is channelled into the tube (Canon 1970; Kalkofen et al. 1989). This leads to an enhancement of the vertical radiative flux, which increases with the degree of evacuation and consequently increases with a decrease in β_0.

We now turn to the variation of β with z for various values of β_0. From equation (2) it is easy to see that β is constant with depth if $T_i = T_e$ at every z. In general, since the internal and external temperatures are almost the same at each geometric level in the upper layers of the tube, we expect β to be nearly constant with z in this region. At $z \approx 0$, owing to the tube being hotter than its surroundings, we expect a small increase in β close to this level. For $z > 0$, the tube is cooler than the outside, due to the effect of reduced convective efficiency in the tube, and this leads to a slight decrease of β with z.

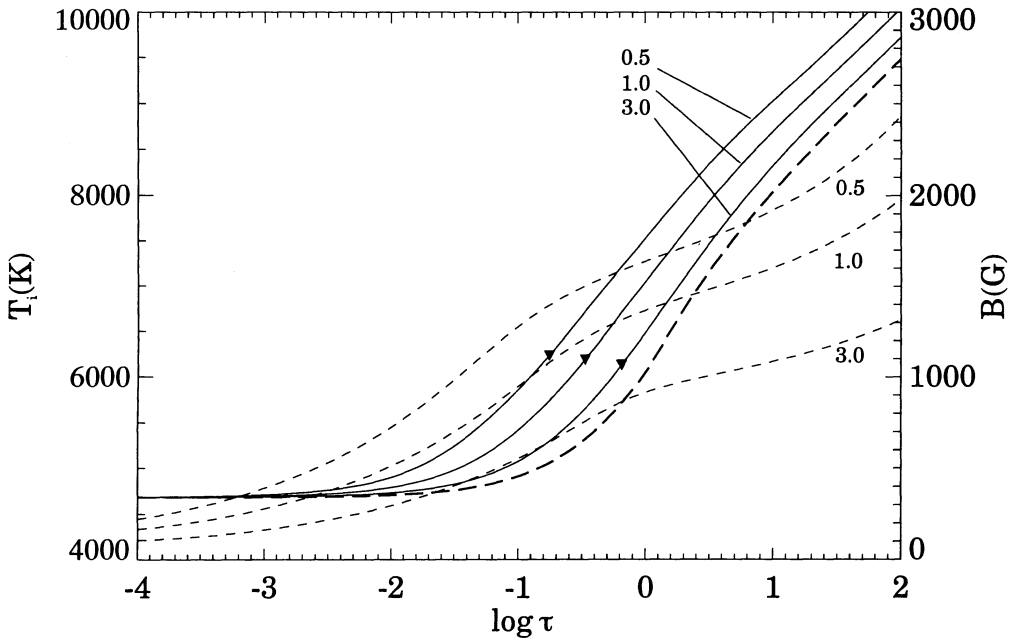

FIG. 5.—Variation with log τ of T_i (*solid lines*) and B (*dashed lines*) for different values of β_0 for $\alpha = 0.2$ and $a(0) = 50$ km. The thick dashed line denotes the run of T_e with optical depth in the external atmosphere. The filled inverted triangles denote $z = 0$.

4.7. *Influence of α on the Temperature and Vertical Flux in the Tube*

Figure 7 shows the effect of changes in the efficiency of convection in the tube on the internal temperature and the net vertical energy flux distributions as functions of the internal optical depth, for two values of α, 0.2 and 0.8, assuming $\beta_0 = 1.0$ and $a(0) = 50$ km. Changing α from 0.2 to 0.8 has almost a negligible effect on the temperature distribution (*solid curves*). In the photospheric layers and above, this is obvious because the dominant transport mechanism is radiation. However, in the deeper layers, where radiative energy transport is negligibly small (owing to the extremely large opacity), we have a flux-conserving atmosphere. Therefore, the energy equation can be integrated with respect to z to yield

$$F_{c,z} = F_{\rm tot} = F_{\rm bot} = \alpha F_{\odot} ,$$

where we have assumed that the horizontal component of the convective flux is zero. Thus, varying α essentially alters the value of the total vertical flux in the convection-dominated part of the atmosphere (which must be constant), as can be

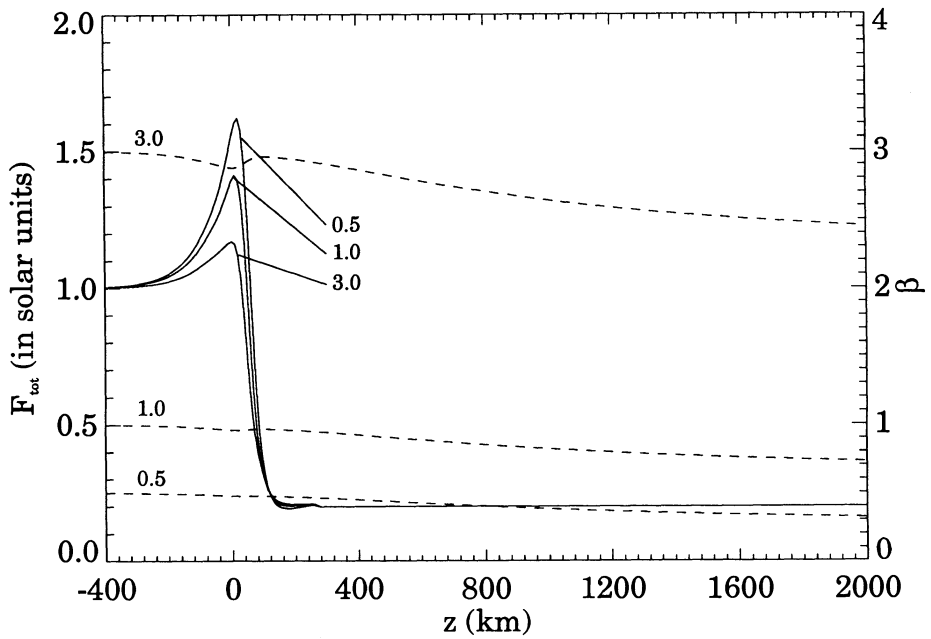

FIG. 6.—Variation with z of $F_{\rm tot}$ (*solid lines*) and β (*dashed lines*) for different values of β_0 for $\alpha = 0.2$ and $a(0) = 50$ km

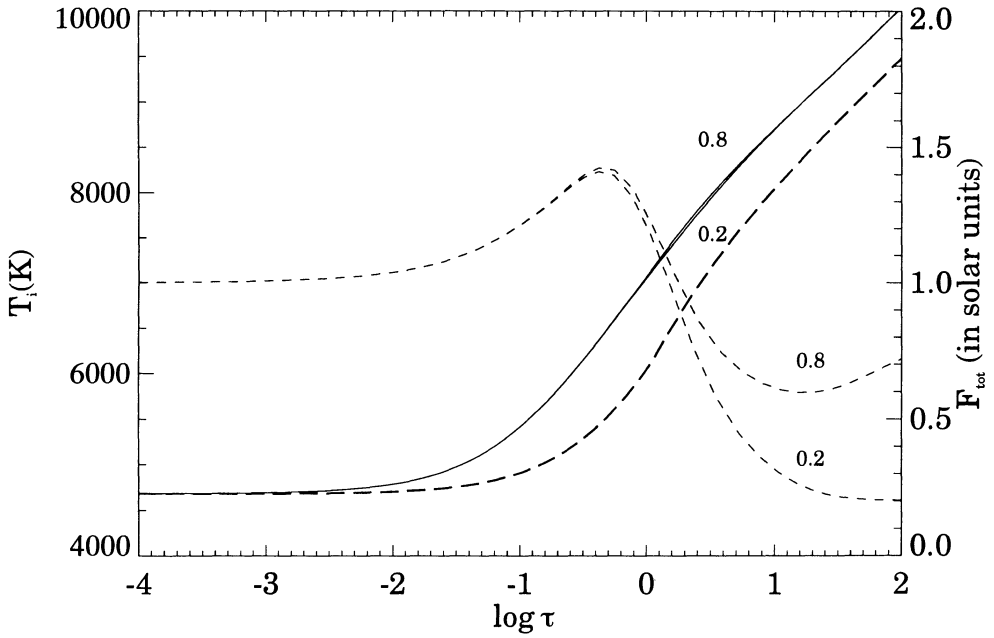

FIG. 7.—Variation of T_i (*solid lines*) and F_{tot} (*dashed lines*) with log τ for different values of α for $\beta_0 = 1.0$ and $a(0) = 50$ km

seen from the dashed curves in the figure, corresponding to F_{tot}. However, since the latter depends upon a high power of T, changing the energy flux by a factor of 4 leads to only a small change in the internal temperature of the tube. It should also be noted that the departure of the total vertical flux from a constant value demonstrates the importance of two-dimensional effects (due to radiative heat exchange between the tube and the surrounding medium).

5. DISCUSSION

5.1. *Treatment of Radiative Transfer*

The purpose of the present investigation was to improve the earlier analysis used in Paper I by using a more realistic treatment of radiative transfer. In Paper I, radiative transfer was modeled using the Unno-Spiegel generalization of the Eddington approximation, as adapted to a thin flux tube. Although this method allows both vertical and horizontal heat transport to be considered, its validity, particularly in the optically thin layers, is questionable. We found from § 4.3, by a comparison with a more careful treatment of transfer using a multistream approximation, that the generalized Eddington approximation overestimates the effect of lateral heat exchange in the optically thin part of the atmosphere, by giving essentially identical internal and external temperatures. However, in the optically thick layers, this approximation is much better. From a computational point of view, the calculation in the multistream approximation is much more cumbersome than that in the Eddington approximation, as each iteration involves solving the transfer equation along $3N$ rays. Furthermore, since it is not practical to linearize J, the convergence is much slower than that obtained in Paper I. Another difference with Paper I is that we do not use an additional heating term in the energy equation. This term was used earlier to match the temperature structure in the layers above $z = 0$ with empirical models. However, from a physical point of view it is difficult to justify the extra energy input being the cause of the temperature discrepancy with empirical models; this more likely reflects the error in the angle and gray approximations. Indeed, increasing the number of angles, as we have seen from Figure 1, leads to a higher temperature in the photospheric layers. This effect saturates for three or more angles. Although the temperature is still somewhat lower than that of the empirical models (the maximum difference is less than 300 K), we decided, nevertheless, not to include the additional energy heating in our models.

A relevant question in the present context is how the radiative transfer accounts for the cylindrical geometry. It would appear that the results we have obtained would also be valid on the axis of a flux sheath, with the same horizontal and vertical variations of physical variables. This appears to be true, in the special cases that we have treated of tubes, which are sufficiently thin and where the internal atmosphere varies linearly with horizontal distance from the axis. However, in general, this is not valid, particularly away from the axis, so that the azimuthal variation needs to be explicitly taken into account. Let us now try and assess the error made in using a single planar cut to compute the mean radiation intensity on the tube axis. Figure 8 shows the variation with z of $\Delta J_{i,0}/J_{i,r}$, [assuming default parameters except for $a(0) = 100$ km], where $\Delta J_{i,0} = J_i(z, 0) - J_i(z, r)$, $J_{i,0} \equiv J_i(z, 0)$, and $J_{i,r} \equiv J_i(z, r)$. The latter is the mean intensity on the axis of a tangential plane at a radial distance r from the tube axis. The axial intensity was computed using a single plane, whereas for the off-axis intensity, we used four equidistant planar cuts, which were then used to resolve the azimuthal variation. In Figure 8, the two curves correspond to different locations of the outermost tangential plane (whose distances in kilometers from the tube axis are denoted by the numbers beside the curves). We find that the maximum difference in the mean intensities does not exceed 3% at any value of z, which corresponds to an infinitesimal change in the temperature. Increasing, the number of tangential cuts above four does not have any discernible influence on the results. It thus appears that for the case of thin flux tubes that we have examined, using a single plane to compute the mean radiation field appears to be justified.

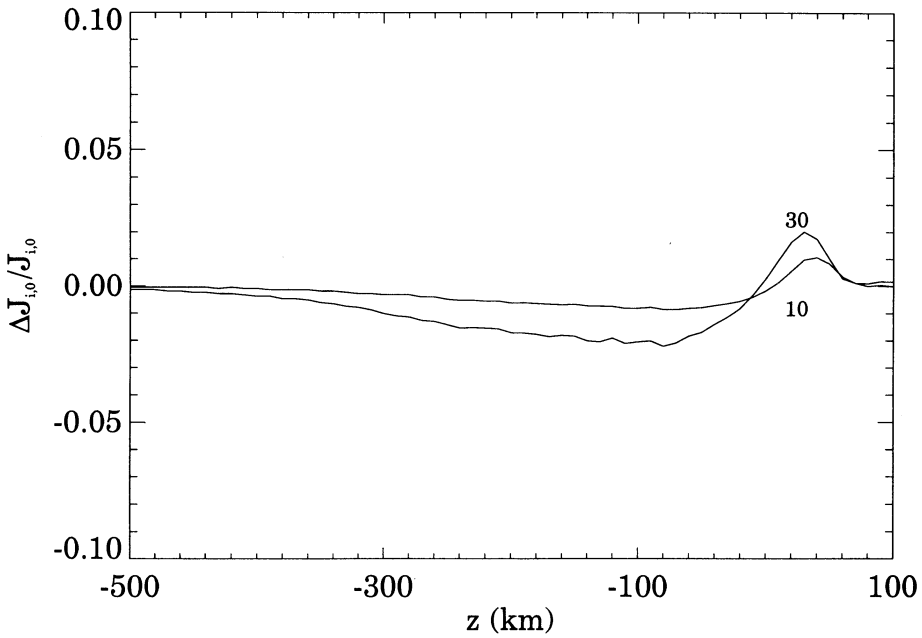

FIG. 8.—Variation of $\Delta J_{i,0}/J_{i,0}$ with z for two different locations of the radial distance (in km) from the tube axis (used to label the curves) at which the off-axis mean intensity is calculated, assuming $\beta_0 = 1.0$ and $a(0) = 50$ km.

5.2. *Comparison with Semiempirical Models*

It is useful to compare our results with those of semiempirical models. Figure 9 shows theoretical internal temperature profiles as functions of optical depth in the flux tube (*solid curves*), denoted by *a* and *b* corresponding to $\beta_0 = 1.0$ and $\beta_0 = 0.5$, respectively. The dotted and dashed lines correspond to the network and plage models of Solanki & Brigljevic (1992) (hereafter SB), whereas the vertical bars denote the range of temperatures for various semiempirical models computed by Zayer et al. (1990). It is clear that for $\log \tau < -2$, the theoretical models are somewhat cooler than the SB models and fall on the lower range of the Zayer et al. (1990) models. For $-2 < \log \tau < -0.5$, model *b*, corresponding to $\beta_0 = 0.5$, appears to lie within the range of the semiempirical models, but model *a* is still too cool. However, for $-0.5 < \log \tau < 1$, model *a* exhibits better agreement with semiempirical models (excluding the plage model), whereas model *b* appears to have somewhat higher temperaures in layers greater than optical depth unity. In these layers, both models are much hotter than the SB plage model.

Table 1 shows various quantities for four values of β_0 and different values of $a(0)$, the radius at $z = 0$. The magnetic flux is denoted by Φ, and z_W is the Wilson depression in the tube, i.e., the geometric depth corresponding to optical depth unity. The corresponding temperature and magnetic field strength are denoted by T_W and B_W. Finally, the last column denotes the intensity contrast η of the tube with respect to its surroundings. This was calculated by determining the ratio of the emergent internal and external intensities at the top of the computational domain for a vertical ray. Owing to numerical difficulties associated with problems of convergence, the full range of $a(0)$ values could not be considered for models with $\beta_0 = 0.1$ and $\beta_0 = 0.5$.

We find that the temperatures corresponding to $\beta_0 = 1.0$ agree better with semiempirical models. The models corresponding to $\beta_0 = 0.5$ and $\beta_0 = 0.1$ are too hot. On the other hand, the field strength found from semiempirical models favors a value close to $B = 2000$ G (Zayer et al. 1990), which would suggest a value of β_0 close to $\beta_0 = 0.1$. However, the temperature discrepancy for such low values of β_0 would be even worse. On theoretical considerations, there appears to be no known physical mechanism that could yield such large field strengths in intense flux tubes. Convective collapse, which is widely thought to be the process for concentrating the photospheric field to kilogauss stregnths, generally produces fields of around 1300–1400 G at $\tau = 1$ (Hasan 1984, 1985).

Let us now turn to a comparison of the intensity contrast η with semiempirical models. For network models, SB find that η is in the range 1.1–1.5. This agrees better with the models corresponding to $\beta_0 = 1.0$ than with $\beta_0 = 0.5$. The agreement would be even better for larger values of β_0, but then the discrepancy between the field strength from theoretical and semiempirical models would be even worse. The contrast values for $\beta_0 = 1.0$ are in good agreement with those found by Koutchmy (1977), viz., $\eta \approx 1.6$–2.0. These were derived from intensity measurements and image restoration. A similar range of values was found by Muller & Keil (1983) and Auffret & Muller (1991). In the method of SB, only properties of the flux tube enter the determination of the contrast, while the intensity measurements have contributions from the ambient medium, owing to the limitations of spatial resolution. Thus, the values based upon the latter method give lower limits to the true flux tube intensity, although being somewhat higher than those found by SB. We should also point out that the values of η given in Table 1 are broadly similar to those calculated theoretically by Grossman-Doerth et al. (1989) for a tube with slab geometry.

In plages, SB find η less than 1 (typically ≈ 0.85), which is in disagreement with our calculations. The reason for this could possibly lie in the fact that plages may contain, in addition to facular points, a substantial number of small pores not detectable using Fourier transform spectroscopy (FTS) with low spatial resolution. As SB have pointed out, their determination of η is an average over all magnetic features contained in the

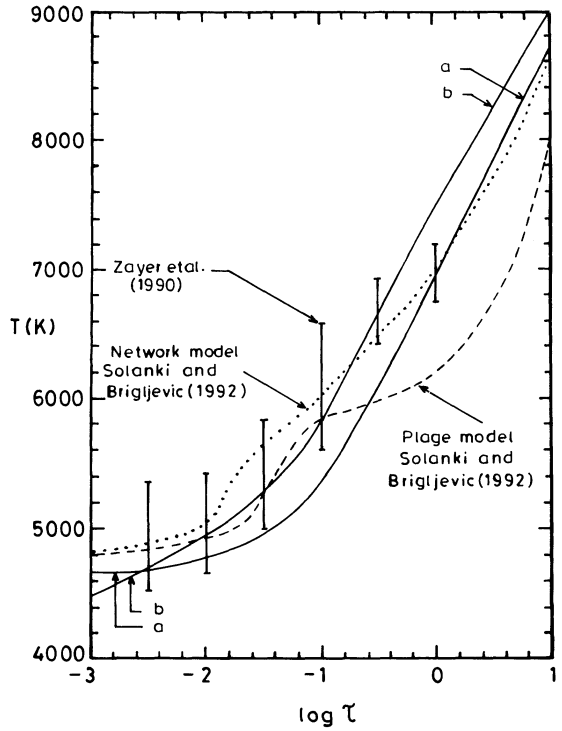

FIG. 9.—Comparison with semiempirical models of the theoretically computed temperature profiles (*solid lines*) in the tube as a function of the internal optical depth for $\beta_0 = 1.0$ (curve *a*) and $\beta_0 = 0.5$ (curve *b*), assuming $\alpha = 0.2$ and $a(0) = 50$ km. The dotted and dashed lines correspond to the network and plage models of Solanki & Brigljevic (1992). The vertical bars denote the range of values in the Zayer et al. (1990) models.

field of view of the observation. It appears, therefore, that there are some uncertainties regarding the observational determination of the continuum contrast of small-scale flux tubes (see also the discrepancy between the results of SB and those of Schüssler & Solanki 1988). Very high spatial resolution (less than 0".5) would be desirable to settle this question.

5.3. *Influence of the Sudden Turn-on of Convection*

In § 1 we mentioned that equilibrium two-dimensional flux-tube models, with radiation and convection operating in different layers, have been constructed by Pizzo et al. (1993). Actually, the convective flux in their models is zero, since they assume an adiabatic temperature stratification in layers where the Schwarzschild criterion for the onset of convection is satisfied. This is at best an approximation to the real situation, since, even though the magnetic field is likely to reduce the efficiency of convective energy transport within the tube, it seems unlikely that convection will be totally suppressed, at least in the regions close to optical depth unity. Let us consider the artificial situation in which we allow radiation and convection to operate in separate layers and examine how the atmosphere determined in this way differs from one in which both mechanisms operate simultaneously. Figure 10 examines the influence of the sudden turn-on of convection on the internal temperature of a flux tube. The solid curves, denoted by *a* and *b* correspond respectively to continuous and discontinuous transitions between predominantly radiative transport and convective transport, for $\alpha = 0.2$, $\beta = 1.0$, and $a(0) = 200$ km. The dashed and dotted curves denoted the temperature distributions corresponding to curves *a* and *b*, respectively. We locate the transition layer z_{tran} for case *b* just below the level at which the Schwarzschild criterion is satisfied. For consistency, we follow this prescription also for the external atmosphere. In the calculations, z_{tran} was 20 km and 50 km, respectively, for the external and internal atmospheres. The inverted triangles denote the Wilson depressions in the tube, located at $z = 41$ km and $z = 47$ km, respectively, for models *b* and *a*. We find that the models with the discontinuous transition are significantly hotter in the layers below $z = 0$ and have an intensity

TABLE 1

VARIOUS QUANTITIES IN A FLUX TUBE FOR DIFFERENT VALUES OF β_0 AND a_0

β_0	$a(0)$ (km)	Φ (Mx)	z_W (km)	T_W (K)	B_W (G)	η
0.1.....	50	1.4×10^{17}	90	8789	2104	4.04
0.1.....	100	5.5×10^{17}	94	8786	2127	4.04
0.5.....	50	1.2×10^{17}	52	7526	1638	2.21
0.5.....	100	4.8×10^{17}	55	7483	1664	2.18
0.5.....	200	1.9×10^{18}	63	7468	1769	2.18
1.0.....	50	1.0×10^{17}	37	7024	1360	1.71
1.0.....	100	4.1×10^{17}	41	7014	1393	1.69
1.0.....	200	1.6×10^{18}	47	6990	1442	1.69
1.0.....	400	6.6×10^{18}	55	6975	1504	1.68
3.0.....	50	7.3×10^{16}	18	6482	914	1.25
3.0.....	100	2.9×10^{17}	21	6456	933	1.24
3.0.....	200	1.2×10^{18}	24	6423	966	1.23
3.0.....	400	4.7×10^{18}	28	6394	1001	1.22

NOTE.—T_W and B_W are the temperature and magnetic field values at the Wilson depression z_W.

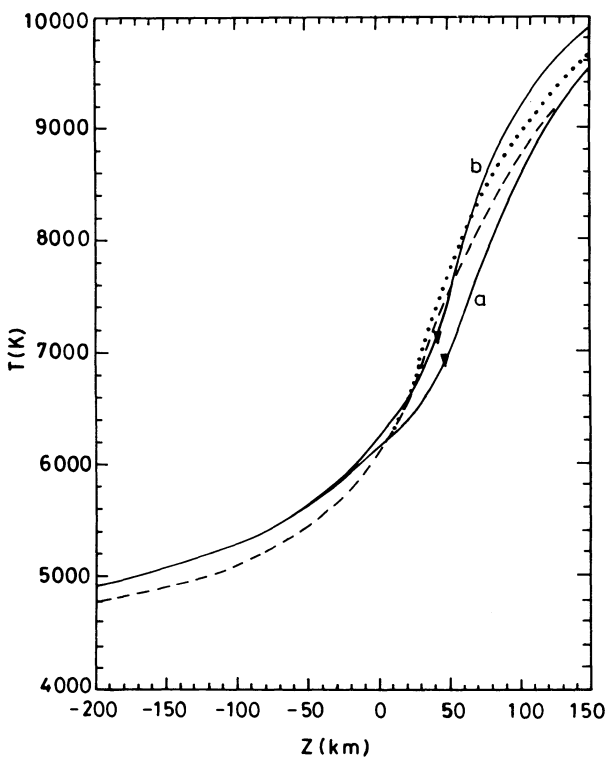

FIG. 10.—Comparison of T_i as a function of z (*solid lines*) for continuous (curve *a*) and discontinuous transitions (curve *b*) between radiative and convective energy transport, for $\beta_0 = 1.0$ and $a(0) = 200$ km. The filled inverted triangles denote the locations where the optical depth is unity. The dashed and dotted curves denote the variation of T_e corresponding to cases *a* and *b*, respectively. The corresponding transition levels for case *b* are at $z = 20$ km and $z = 50$ km for the external and internal atmospheres, respectively.

contrast which is about 12% higher than that of the continuous models. We also find that the differences are further enhanced for thicker flux tubes. For instance, when $a(0) = 400$ km, the error in the contrast is about 20%. Physically, this is understandable because as the radius of the tube increases, heat exchange between the tube and its surroundings becomes ineffective close to $z = 0$. In the layers for which $\tau > 1$, the vertical radiative flux cannot be entirely balanced by the lateral radiative flux, owing to the sharp rise of opacity and, consequently, a nonvanishing vertical convective flux is required to conserve energy. As the tubes become thicker, the transition layer where the radiative and convective fluxes have comparable magnitudes also becomes bigger, leading to the discrepancy mentioned above.

5.4. *Limitations of the Thin Flux-Tube Approximation*

Let us briefly comment on the limitations of equilibrium solutions, using the thin flux-tube approximation. Broadly speaking, our results can only be applied to tubes which are sufficiently narrow, so that the magnetic tension forces can be neglected. Steiner & Pizzo (1989) found that for tubes with $a(0) \leq 100$ km, the field lines computed using the exact magnetostatic and thin flux-tube solutions were practically indistinguishable. For thicker tubes, however, the neglect of the tension led to the radius, computed using the thin flux tube approximating, being overestimated. The error in radius for a tube with $a(0) = 200$ km was about 15% at $z = -500$ km but almost negligible for $z \leq -200$ km. Another inherent assumption in the present treatment is that we neglect the effect of the flux tube on the surroundings. In reality, the presence of the flux tube will influence energy transport in its immediate surroundings. The main effect of this is a cooling of the adjacent exterior and the generation of a circulation flow there (Deinzer et al. 1984, Grossmann-Doerth et al. 1989).

5.5. *Stability of Flux-Tube Models*

Lastly, let us briefly discuss the stability of our models. Owing to the expansion of the tubes with height, the magnetic field lines are concave with respect to the ambient medium. It is well known that such a configuration is susceptible to the flute or interchange instability. Meyer, Schmidt, & Weiss (1977) showed that if the tubes are sufficiently thick, then this instability can be stabilized by buoyancy. However, for thin tubes some other mechanism is needed, such as a whirl flow around the tube (Schüssler 1984). The magnitude of the whirl velocities needed for stabilization for flux tubes in the solar atmosphere has been studied in some detail by Bünte, Steiner, & Pizzo (1993), and Bünte, Hasan, & Kalkofen (1993). In addition to the interchange instability, there is also the question of convective stability of the present models. On the basis of earlier linear adiabatic studies (Spruit & Zweibel 1979) the instability can be suppressed for a flux tube (with the same temperature stratification as the external medium) for $\beta \leq 1.5$. However, the presence of heat exchange between the tube and the ambient medium, could lead to overstable oscillations, no matter how strong the field (Hasan 1986). We defer a thorough examination of this problem to a subsequent investigation.

6. CONCLUSIONS

We have computed static equilibrium models of intense flux tubes in the solar atmosphere for a wide range of input parameters. On the basis of our investigation, we can draw a number of important conclusions. These are the following:

1. The thermodynamic properties of the flux-tube atmosphere are very sensitive to radiative energy transport in the photospheric layers of the tube. Therefore, care is needed in the treatment of radiative transfer to accurately model the atmosphere in the tube.
2. At equal geometric levels, the atmosphere in the tube is generally hotter in the photosphere and cooler in the convection zone than the ambient medium. This temperature difference increases as the tube becomes thicker. However, at equal optical depths, the tubes are always hotter than their surroundings.
3. The total vertical energy flux on the axis of a tube is not constant with height, but increases from the convection zone to the photosphere. The maximum occurs at the base of the photosphere. On the other hand, β exhibits only a weak height dependence.
4. The stratification in the tube is fairly insensitive to the convective efficiency parameter α. However, it does depend upon whether there is a continuous or abrupt transition of energy transport from radiation to convection.
5. A comparison with semiempirical models shows that the theoretically computed temperature profiles and the intensity contrast are in broad agreement for network models, but the magnetic field strengths are somewhat lower. Models which have larger field strengths are too hot compared with observations.

In summary, we have attempted to provide equilibrium models of flux tubes which can be used as inputs for more extensive studies involving linear stability and time-dependent behavior. Also, we expect that the sophistication of radiative transfer is sufficient to make meaningful comparison with observations.

We are grateful to F. Kneer for carefully reading the manuscript and for providing helpful comments. We are also thankful to O. Steiner for valuable advice, particularly on treating the azimuthal variation of the radiation field. The work of S. S. H. was supported by the Smithsonian Astrophysical Observatory, by NASA through grant NAGW-1568, and by the NSF under the US-India Cooperative Science Program. His travel between India and the US was supported by a grant from the IAU.

REFERENCES

Auer, L. H., & Mihalas, D. 1968, ApJ, 151, 311
Auffret, H., & Muller, R. 1991, A&A, 246, 264
Bünte, M., Hasan, S. S., & Kalkofen, W. 1993, A&A, in press
Bünte, M., Steiner, O., & Pizzo, V. J. 1993, A&A, 273, 287 in press
Canon, C. J. 1970, ApJ, 161, 221
Chandrasekhar, S. 1960, Radiative Transfer (New York: Dover)
Cox, J. P., & Guili, R. T. 1968, Principles of Stellar Structure, Vol. 1 (New York: Gordon & Breach)
Deinzer, W., Hensler, G., Schüssler, M., & Weishaar, E. 1984, A&A, 139, 435
Dunn, R. B., & Zirker, J. B. 1973, Sol. Phys., 33, 281
Fabiani Bendicho, P., Kneer, F., & Trujillo Bueno, J. 1992, A&A, 264, 229
Ferrari, A., Massaglia, S., Kalkofen, W., Rosner, R., & Bodo G. 1985, ApJ, 298, 181
Grossmann-Doerth, U., Kneer, F., & v. Uexküll, M. 1974, Sol. Phys., 37, 85
Grossmann-Doerth, U., Knölker, M., & Schussler, M. 1989, in Solar and Stellar Granulation, NATO Advanced Research Workshop, ed. R. J. Rutten & G. Severino (Dordrecht: Reidel), 481
Gustafsson, B. 1971, A&A, 10, 187
Hasan, S. S. 1984, ApJ, 285, 851
———. 1985, A&A, 143, 39
———. 1986, MNRAS, 219, 357
———. 1988, ApJ, 332, 499

Hasan, S. S. 1990, in Am. Geophys. Union Monog. 58, Physics of Magnetic Flux Ropes, ed. C. T. Russell, E. R. Priest & L. C. Lee, 157
———. 1991, in Chromospheric and Coronal Heating Mechanisms, ed. P. Ulmschneider, E. R. Priest & R. Rosner (Berlin: Springer-Verlag), 408
Kalkofen, W., Bodo, G., Massaglia, S., & Rossi, P. 1989, in Solar and Stellar Granulation, ed. R. J. Rutten & G. Severino (Dordrecht: Kluwer), 571
Kalkofen, W., Rosner, R., Ferrari, A., & Massaglia, S. 1986, ApJ, 304, 519
Keller, C. U., Solanki, S. K., Steiner, O., & Stenflo, J. O. 1990, A&A, 233, 583
Knölker, M., & Schüssler, M. 1988, A&A, 202, 275
Knölker, M., Schüssler, M., & Weisshaar, E. 1988, A&A, 194, 257
Koutchmy, S. 1977, A&A, 99, 111
Kunasz, P. B., & Auer, L. H. 1988, J. Quant. Spectrosc. Rad. Transfer, 39, 67
Kurucz, R. L. 1992, private communication
Mehltretter, J. P. 1974, Sol. Phys., 28, 43
Meyer, F., Schmidt, H. U., & Weiss, N. O. 1977, MNRAS, 179, 741
Mihalas, D. 1978, Stellar Atmospheres (2d ed.; San Francisco: Freeman)
Muller, R., & Keil, S. L. 1983, Sol. Phys., 87, 243
Pizzo, V. J., MacGregor, K. B., & Kunasz, P. B. 1993, ApJ, 413, 764
Roger, F. J., & Iglesias, C. 1992, ApJS, 79, 507
Schüssler, M. 1984, A&A, 140, 453
Schüssler, M., & Solanki, S. K. 1988, A&A, 192, 338
Solanki, S. K. 1990, in IAU Symp. 138, Solar Photosphere, Structure, Convection and Magnetic Fields, ed. J. O. Stenflo (Dordrecht: Kluwer), 103
Solanki, S. K., & Brigljevic, V. 1992, A&A, 262, L29
Spruit, H. C. 1976, Sol. Phys., 50, 269
———. 1977, Ph.D. thesis, Univ. of Utrecht
Spruit, H. C., & Zweibel, E. 1979, Sol. Phys., 62, 15
Steiner, O., & Pizzo, V. J. 1989, A&A, 211, 411
Steiner, O., & Stenflo, J. O. 1989, in IAU Symp. 138, Solar Photosphere, Structure, Convection and Magnetic Fields, ed. J. O. Stenflo (Dordrecht: Kluwer), 181
Stenflo, J. O. 1989, A&A, Rev., 1, 3
Stone, J. M., Mihalas, D., & Norman, M. 1992, ApJS, 80, 819
Title, A. M., Topka, K. P., Tarbell, T. D., Schmidt, W., Balke, C., & Scharmer, G. 1992, ApJ, 393, 782
Vernazza, J. E., Avrett, E. H., & Loeser, R. 1976, ApJS, 30, 1
Zayer, I., Solanki, S. K., Stenflo, J. O., & Keller, C. U. 1990, A&A, 239, 366